Optics Letters

High-power, high-repetition-rate tunable longwave mid-IR sources based on DFG in the OPA regime

Yang Liu,[1,2] Jimin Zhao,[1,2,3] Zhiyi Wei,[1,2,3] Franz X. Kärtner,[4] and Guoqing Chang[1,2,3,*]

[1] Beijing National Laboratory for Condensed Matter Physics, Institute of Physics, Chinese Academy of Sciences, Beijing 100190, China
[2] University of Chinese Academy of Sciences, Beijing 100049, China
[3] Songshan Lake Materials Laboratory, Dongguan, Guangdong 523808, China
[4] Center for Free-Electron Laser Science, Deutsches Elektronen-Synchrotron, Notkestraße 85, 22607 Hamburg, Germany
*Corresponding author: guoqing.chang@iphy.ac.cn

Received 1 December 2022; revised 11 January 2023; accepted 15 January 2023; posted 17 January 2023; published 14 February 2023

We demonstrate high-power longwave mid-IR ultrafast sources based on a high-power Er-fiber laser system at 1.55 µm with a 32-MHz repetition rate. Compared with previous 1.03-µm-driven difference frequency generation (DFG), our current configuration allows tighter focusing in the GaSe crystal thanks to an increased damage threshold at 1.55 µm. Consequently, the 1.55-µm-driven DFG can operate in the regime of optical parametric amplification (OPA), in which the mid-IR power grows exponentially with respect to the square root of the pumping power. We experimentally demonstrate this operation regime and achieve broadband mid-IR pulses that are tunable in the 7.7–17.3 µm range with a maximum average power of 58.3 mW, which is also confirmed by our numerical simulation.

https://doi.org/10.1364/OL.482461

High repetition-rate (>10 MHz) femtosecond laser sources that are tunable in the longwave mid-IR range of 6–20 µm (known as the molecular "fingerprint" region) and have high average power (>10 mW) hold promise for many important spectroscopic applications [1–4]. These mid-IR sources are usually derived from a high-power near-IR femtosecond laser ("source laser") using difference-frequency generation (DFG). In a typical DFG configuration, one portion of the near-IR laser pulses serves as pump pulses; the other portion is employed to generate wavelength-tunable signal pulses centered at a longer wavelength via nonlinear wavelength conversion. DFG between the pump and signal pulses produces tunable mid-IR pulses. Due to rapid advances in ultrafast fiber optic technology, high-power ultrafast fiber lasers have been widely adopted as source lasers, and fiber-optic nonlinearities are employed to derive the signal pulses [5–8].

Many groups have employed the fiber-optic soliton self-frequency shift [5,9–11] and supercontinuum generation [6,12–19] to generate the signal pulses; however, the pulse energy is typically less than 1 nJ. The use of these low-energy signal pulses in DFG inevitably leads to low-energy (and low average power) mid-IR pulses, which severely limits their practical spectroscopic applications. The key to power scaling a DFG-based mid-IR source is to generate high-energy signal pulses that are tunable in a broad wavelength range. For example, Lee *et al.* used Tm-doped fiber to amplify the signal pulses—which were generated by supercontinuum generation and centered at 1.8–1.96 µm—to a pulse energy of 6.4 nJ; the resulting mid-IR pulses had a repetition rate of 93.4 MHz with a maximum average power of 69 mW [6]. However, due to limited gain bandwidth of the Tm-doped fiber, the generated mid-IR pulses exhibit a limited tuning range of 6–11 µm. We proposed an alternative fiber-optic method to produce broadly tunable, energetic femtosecond pulses. In this method, a short piece of optical fiber with a small dispersion is used to host the spectral broadening, which is largely caused by self-phase modulation (SPM). Consequently, the broadened spectrum consists of several isolated spectral lobes, and filtering the outermost lobes produces nearly transform-limited pulses. This method is dubbed SESS: SPM-enabled spectral selection [20]. SESS exhibits excellent energy scalability; using large-mode-area fiber with a short length (<10 cm) generated SESS pulses with up to 100 nJ of energy [21]. In 2018, we demonstrated a tunable mid-IR frequency comb based on an Yb-fiber laser with the signal pulse derived via SESS [3]. More specifically, the pump pulse centers at 1.03 µm, the signal pulse is tunable in the range of 1.1–1.2 µm, and their DFG in GaSe produces mid-IR pulses tunable from 7 to 18 µm with up to 5.4 mW of average power [7]. Further power scaling is limited by a large pump–signal group-velocity mismatch (GVM) and the low damage threshold of GaSe at 1.03 µm. In this Letter, we demonstrate longwave mid-IR sources based on a high-power Er-fiber laser at 1.55 µm with signal pulses derived via SESS. The average power of the longwave mid-IR source is increased by one order of magnitude compared with our previous work based on Yb-fiber lasers. We also demonstrate that DFG operates in the optical parametric amplification (OPA) regime thanks to an increased nonlinear interaction.

When we replace the Yb-fiber laser by an Er-fiber laser to drive DFG in GaSe, the increased pump/signal wavelength immediately leads to three advantages. (1) The GaSe has a bandgap of ~2.1 eV and exhibits strong two-photon absorption for pulses with a center wavelength shorter than ~1.18 µm. Thus, the crystal damage threshold strongly depends on the

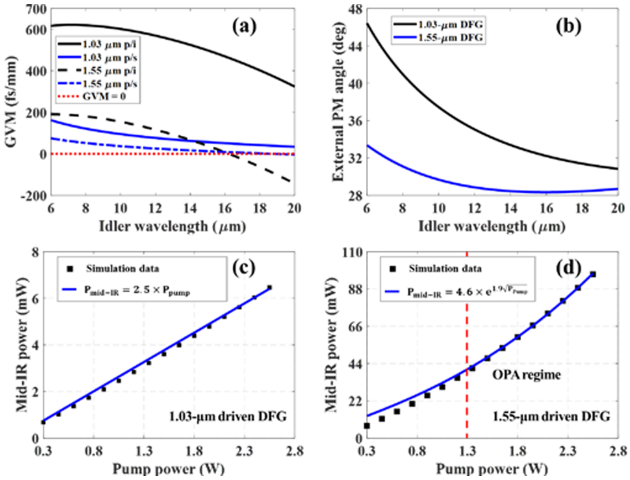

Fig. 1. Comparison between 1.03-μm-driven DFG and 1.55-μm-driven type-I DFG inside GaSe. (a) GVM, (b) external phase-matching angle, and (c), (d) power scaling of 10-μm mid-IR pulses.

pulse wavelength. At an ∼30-MHz repetition rate, we experimentally found that the damage threshold is about 3 GW/cm^2 for ∼300-fs pulses at 1.03 μm [7]; however, the damage threshold is greater than 25 GW/cm^2 at 1.55 μm. (2) Figure 1(a) shows that GVMs are significantly reduced to generate mid-IR pulses tunable in the wavelength range of 6–20 μm. Such reduced GVMs improve the interaction distance and benefit energy conversion in the DFG. (3) Figure 1(b) shows that, compared with 1.03-μm-driven DFG, the external phase-matching angle corresponding to the 1.55-μm-driven DFG varies over a much smaller range. Especially when generating mid-IR pulses tunable from 10 to 20 μm, the crystal orientation remains nearly constant, which relaxes the requirement to finely rotate the GaSe to achieve phase matching.

To directly show the advantages of 1.55-μm-driven DFG over 1.03-μm-driven DFG, we carry out a numerical study using the coupled wave equations [22]. We simulate the type-I DFG process in a 2-mm-thick GaSe crystal that generates mid-IR pulses centered at 10 μm with the pump pulses centered at 1.03 μm or 1.55 μm. For simplicity, all pulses are assumed to be 290 fs in duration (full width at half maximum) with a sech^2 profile. Table 1 lists other simulation parameters. To match the subsequent experimental implementation, we assume that the GaSe crystal has no anti-reflection coating, and thus we include in the simulation the Fresnel reflection losses at both crystal facets. In a previous theoretical study, we identified two operation regimes—the linear regime and the OPA regime—depending on the nonlinear interaction strength of DFG in GaSe [22]. Figures 1(c) and 1(d) compare the power scaling of the mid-IR pulses produced by 1.03-μm-driven DFG and 1.55-μm-driven DFG as a function of pump power with the signal power fixed at 225 mW, respectively. For the 1.03-μm-driven DFG [Fig. 1(c)], the good overlap between simulation data [squares in Fig. 1(c)] and the linear fitting curve [solid line in Fig. 1(c)] shows that the DFG operates in the linear regime. This regime corresponds to a weak nonlinear interaction and the mid-IR power increases linearly (or quasi-linearly) with respect to the pump power. At the maximum pump power of 2.55 W (peak intensity in GaSe is ∼1.5 GW/cm^2), the mid-IR power is 6.5 mW. For the 1.55-μm-driven DFG, the much higher damage threshold of GaSe

Table 1. Simulation Parameters for Type-I DFG in 2-mm GaSe

	1.03-μm-Driven DFG	1.55-μm-Driven DFG
Repetition Rate	32 MHz	32 MHz
Pump Wavelength	1.03 μm	1.55 μm
Pump Power	0.3–2.55 W	0.3–2.55W
Signal Wavelength	1.15 μm	1.84 μm
Signal Power	225 mW	225 mW
Focus Diameter	150 μm	50 μm

allows a smaller focus (50 μm versus 150 μm) that results in much stronger nonlinear interaction. As theoretical work predicts, the mid-IR power increases exponentially with respect to the square root of the pump power for DFG working in the OPA regime [22,23]. The solid fitting curve in Fig. 1(d) expresses such a dependence of mid-IR power on pump power. Clearly, when the pump power exceeds 1.3 W [marked by the dashed line in Fig. 1(d)], the DFG starts to operate in the OPA regime and the mid-IR pulses can be generated more efficiently. A comparison between Fig. 1(c) and Fig. 1(d) suggests that the mid-IR power can be improved by one order of magnitude as we shift the pump wavelength from 1.03 μm to 1.55 μm.

Guided by the simulation results, we developed such a high-power longwave mid-IR source, as schematically shown in Fig. 2. The home-built high-power Er-fiber laser system has a configuration with a master oscillator power amplifier with a 32-MHz repetition rate. The amplified pulses can be compressed to a duration of 290 fs by a pair of diffraction gratings with 4 W of average power, corresponding to 125 nJ of pulse energy. Our setup can operate in two modes, which can be switched between using a flip mirror (i.e., FM in Fig. 2). With the flip mirror in the optical path (we refer to this as mode 1), the laser output is split into two replicas. One replica serves as the pump and the other replica is coupled into a piece of fiber for SESS. The 9.6-cm-long fiber used here has a mode-field diameter of 4 μm with a dispersion of −1 ps/nm/km at 1.55 μm. The broadened spectrum at the fiber output is separated by a dichroic mirror (DM in Fig. 2), and a long-pass filter (LPF1 in Fig. 2) selects the rightmost spectral lobe serving as signal pulses. The pump pulses and the signal pulses are collinearly combined, with their temporal overlap ensured by an optical delay line. The combined pulses are tightly focused into the GaSe crystal with a beam diameter of ∼50 μm. After passing through another long-pass filter (LPF2 in Fig. 2) with a cutoff wavelength of 4.5 μm, the generated mid-IR beam is then collimated by a 90°-off-axis parabolic mirror with a focal length of 75 mm. A calibrated thermopile

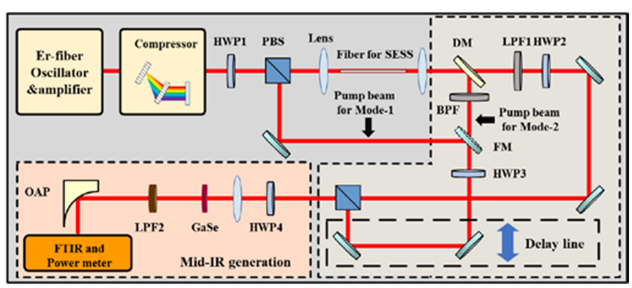

Fig. 2. Schematic setup. HWP: half-wave plate, PBS: polarization beam splitter, DM: dichroic mirror, FM: flip mirror, BPF: bandpass filter, LPF: long-pass filter, OAP: off-axis parabolic mirror.

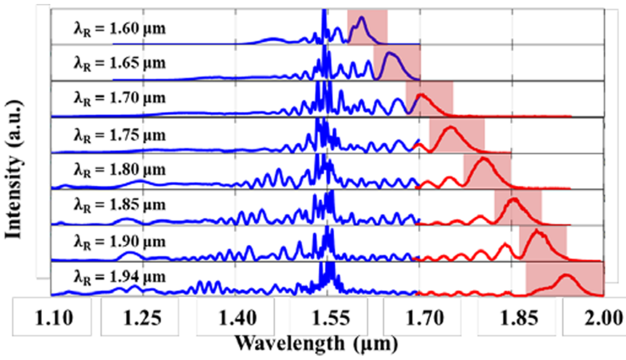

Fig. 3. Spectral broadening, with the rightmost spectral lobe peaking in the range of 1.60–1.94 µm.

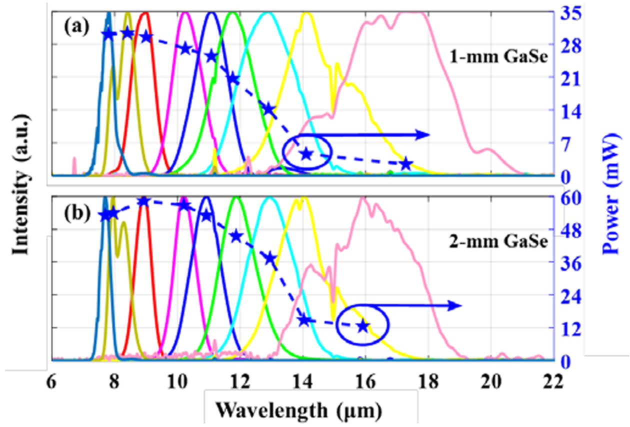

Fig. 4. Measured spectra and average power for mid-IR pulses generated in GaSe with different crystal thicknesses: (a) 1 mm and (b) 2 mm.

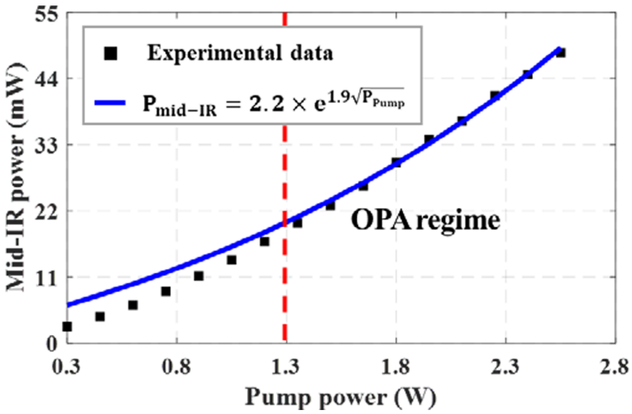

Fig. 5. Scaling of mid-IR power versus pump power with the signal power fixed at 225 mW. Squares: experimental data, solid curve: numerical fit. The dashed curve marks 1.3 W of pump power.

detector measures the average power of the mid-IR pulses, and their optical spectrum is characterized by a Fourier-transform infrared (FTIR) spectrometer.

Figure 3 shows the broadened spectra at the fiber output. The spectra are obtained by stitching measurements using two different optical spectrum analyzers (Yokogawa AQ6370C and Miriad S3). As we increase the coupled power from 0.17 W to 1.17 W, the peak wavelength of the rightmost spectral lobe shifts from 1.6 µm to 1.94 µm. Filtering this spectral lobe by the long-pass filter (LPF1 in Fig. 2) results in wavelength-tunable signal pulses with an average power varying between 50 and 300 mW.

Figure 4(a) plots the measured mid-IR spectra (colored solid curves) and average power (stars) generated from type-I DFG in a 1-mm-thick GaSe crystal. The center wavelength varies from 7.7 to 17.3 µm and the maximum measured power is 30.4 mW for the mid-IR pulses at 8.4 µm as a result of DFG between the pump pulses at 1.55 µm and the signal pulses at 1.90 µm. To scale up the mid-IR power, we replace the 1-mm-thick GaSe crystal by a 2-mm-thick one and redo the experiments. The measured spectra and their average power are presented in Fig. 4(b). Since a thicker crystal permits a smaller phase-matching bandwidth, the mid-IR spectra generated by the 2-mm-thick GaSe crystal have the spectral width reduced by about 10–30% compared with the results obtained using 1-mm GaSe. At the expense of the phase-matching bandwidth, using the thicker GaSe crystal increases the mid-IR power by a factor of 2–5. The minimum average power is 12.5 mW for the mid-IR pulses at 16 µm, and the maximum is 58.3 mW at 8.9 µm, which represents an order of magnitude improvement compared with our previous work based on Yb-fiber laser systems.

To show that this high-repetition-rate DFG operates in the OPA regime, as predicted by the simulation results in Fig. 1(d), we experimentally investigate the scaling of mid-IR power at 10 µm wavelength versus the pump power for type-I DFG in the 2-mm GaSe. To match the simulation, the signal power is fixed at 225 mW, with the pump power increased from 0.3 W to 2.55 W. In Fig. 5, the squares denote the experimental data; the solid fitting curve corresponds to the exponential growth of mid-IR power with respect to the square root of pump power—a characteristic feature of OPA. The results show that the DFG process enters the OPA regime as we increase the pump power beyond 1.3 W [dashed line in Fig. 5], which matches the simulation. However, the measured mid-IR power is only about half of the numerical prediction. Such a discrepancy may be due to the omission of transverse spatial effects (e.g., spatial beam walk-off) in our numerical model. In addition, we use ideal sech^2 pulses rather than real pulses as the simulation input. Nevertheless, the experimental results agree well with the simulation in terms of the overall tendency of the power scaling.

Limited by the tuning range of the rightmost spectral lobe, which is up to ∼1.94 um, the shortest wavelength of the mid-IR pulses is 7.7 µm. In fact, we can use the leftmost spectral lobe as the pump to obtain mid-IR pulses with a broader tuning range. In this operation mode (which we refer to as mode 2), we remove the flip mirror and couple the total average power of 4 W into a dispersion-shifted fiber (DSF) for SPM-enabled spectral broadening. This 9.6-cm-long DSF has a mode-field diameter of 9.6 µm with a dispersion of −8 ps/nm/km at 1.55 µm. In order to make the best use of the laser output power, the negative pre-chirp is added to the pulse before coupling it into the DSF by increasing the grating separation of the compressor (see Fig. 2). The solid curves in Fig. 6 record these output spectra corresponding to different amounts of pre-chirping group-delay dispersion (GDD) added to the input pulse. As the pre-chirp GDD varies from $-32000\ \text{fs}^2$ to $-60000\ \text{fs}^2$, the leftmost (rightmost) spectral lobe can be tuned in the wavelength range of 1.3–1.45 µm (1.6–1.67 µm).

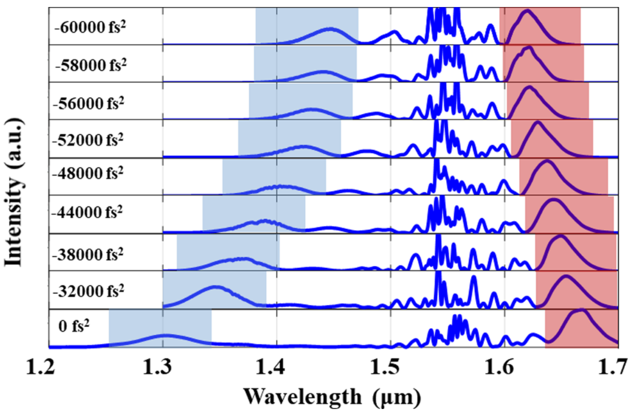

Fig. 6. Spectral broadening in a 9.6-cm DSF with different amounts of negative pre-chirping GDD added to the input pulse.

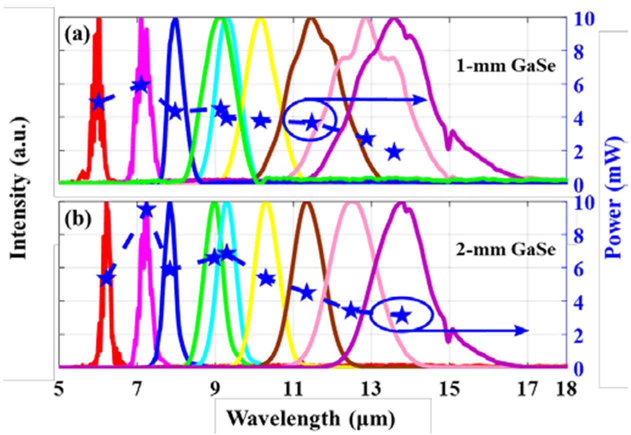

Fig. 7. Measured spectra and average power for mid-IR pulses generated by DFG between the leftmost and rightmost spectral lobes in GaSe crystals with different thicknesses: (a) 1 mm and (b) 2 mm.

Figure 7(a) plots the measured mid-IR spectra (colored solid curves) and average power (stars) generated from the 1-mm-thick GaSe crystal. The center wavelength varies from 6 to 13.6 μm and the maximum measured power is 5.9 mW for the mid-IR pulses at 7.1 μm as a result of DFG between the pump pulses at 1.35 μm and the signal pulses at 1.66 μm. The fine structures in the mid-IR spectrum at about 6 μm and 7 μm are caused by water absorption in the environmental air. To scale up the mid-IR power, we replace the 1-mm-thick GaSe by a 2-mm-thick one and repeat the experiments. The measured spectra and their average power are recorded in Fig. 7(b). The maximum average power is 9.5 mW for the mid-IR pulses at 7.2 μm, and the minimum is 3.1 mW at 13.8 μm.

In conclusion, we have demonstrated high-power longwave mid-IR sources based on a 32-MHz, 1.55-μm Er-fiber laser system. In the first operation mode, the pump pulses are fixed at 1.55 μm and signal pulses tunable in the range 1.60–1.94 μm are obtained using fiber-optic SESS. The DFG in GaSe produces broadband mid-IR pulses that are tunable in the wavelength range of 7.7–17.3 μm and have an average power of up to 58.3 mW. We also demonstrated that the type-I DFG in the 2-mm GaSe operates in the OPA regime when the pump power exceeds 1.3 W. To the best of our knowledge, this constitutes the first experimental demonstration of a high-repetition-rate (i.e., > 30 MHz) DFG source that works in the OPA regime. In the second operation mode, both the pump and signal pulses are derived from SESS, and the resulting mid-IR source is tunable from 6 to 13.6 μm and has up to 9.5 mW of average power. Given that 1.55-μm-driven DFG in GaSe delivers much higher mid-IR power than the 1.03-μm-driven DFG, we anticipate that using a 2-μm Tm-doped ultrafast laser system as the source laser will result in a much greater power improvement. The 2-μm-driven DFG in GaSe features a smaller GVM, less dispersion, a broader phase-matching bandwidth, and a higher crystal damage threshold at the pump wavelength [22]. Consequently, a much larger OPA gain can be achieved, and mid-IR power at the watt level is within reach.

Funding. National Natural Science Foundation of China (62175255, 62227822); The International Partnership Program of Chinese Academy of Sciences (GJHZ1826); National Key Research and Development Program of China (2021YFB3602602).

Disclosures. The method and apparatus reported here has been disclosed as intellectual property by G.Q.C., Y.L., Z.Y.W., and J.M.Z. to the Institute of Physics, Chinese Academy of Sciences, China.

Data availability. Data underlying the results presented in this paper are not publicly available at this time but may be obtained from the authors upon reasonable request.

REFERENCES

1. I. Coddington, N. Newbury, and W. Swann, Optica **3**, 414 (2016).
2. A. Schliesser, N. Picqué, and T. W. Hänsch, Nat. Photonics **6**, 440 (2012).
3. N. Picqué and T. W. Hänsch, Nat. Photonics **13**, 146 (2019).
4. K. C. Cossel, E. M. Waxman, I. A. Finneran, G. A. Blake, J. Ye, and N. R. Newbury, J. Opt. Soc. Am. B **34**, 104 (2017).
5. K. Krzempek, D. Tomaszewska, A. Głuszek, T. Martynkien, P. Mergo, J. Sotor, A. Foltynowicz, and G. Soboń, Opt. Express **27**, 37435 (2019).
6. K. F. Lee, C. J. Hensley, P. G. Schunemann, and M. E. Fermann, Opt. Express **25**, 17411 (2017).
7. G. Zhou, Q. Cao, F. X. Kärtner, and G. Chang, Opt. Lett. **43**, 2953 (2018).
8. X. Su, R. Zhu, B. Wang, Y. Bai, T. Ding, T. Sun, X. Lü, J. Peng, and Y. Zheng, Photonics **9**, 372 (2022).
9. A. Ruehl, A. Gambetta, I. Hartl, M. E. Fermann, K. S. E. Eikema, and M. Marangoni, Opt. Lett. **37**, 2232 (2012).
10. A. Gambetta, N. Coluccelli, M. Cassinerio, D. Gatti, P. Laporta, G. Galzerano, and M. Marangoni, Opt. Lett. **38**, 1155 (2013).
11. J. Sotor, T. Martynkien, P. G. Schunemann, P. Mergo, L. Rutkowski, and G. Soboń, Opt. Express **26**, 11756 (2018).
12. C. R. Phillips, J. Jiang, C. Mohr, A. C. Lin, C. Langrock, M. Snure, D. Bliss, M. Zhu, I. Hartl, J. S. Harris, M. E. Fermann, and M. M. Fejer, Opt. Lett. **37**, 2928 (2012).
13. A. M. Al-Kadry and D. Strickland, Opt. Lett. **36**, 1080 (2011).
14. Y. Yao and W. H. Knox, Opt. Express **20**, 25275 (2012).
15. M. Hajialamdari and D. Strickland, Opt. Lett. **37**, 3570 (2012).
16. Y. Yao and W. H. Knox, Opt. Express **21**, 26612 (2013).
17. D. Sánchez, M. Hemmer, M. Baudisch, K. Zawilski, P. Schunemann, H. Hoogland, R. Holzwarth, and J. Biegert, Opt. Lett. **39**, 6883 (2014).
18. R. Romero-Alvarez, R. Pettus, Z. Wu, and D. Strickland, Opt. Lett. **33**, 1065 (2008).
19. D. G. Winters, P. Schlup, and R. A. Bartels, Opt. Lett. **35**, 2179 (2010).
20. W. Liu, C. Li, Z. Zhang, F. X. Kärtner, and G. Chang, Opt. Express **24**, 15328 (2016).
21. H.-Y. Chung, W. Liu, Q. Cao, L. Song, F. X. Kärtner, and G. Chang, Opt. Express **26**, 3684 (2018).
22. Q. Cao, F. X. Kärtner, and G. Chang, Opt. Express **28**, 1369 (2020).
23. C. Manzoni and G. Cerullo, J. Opt. **18**, 103501 (2016).